
Article:
Wohltmann, I, Lehmann, R, Gottwald, GA et al. (2019) A Lagrangian convective transport scheme including a simulation of the time air parcels spend in updrafts. Geoscientific Model Development Discussions. ISSN: 1991-962X

https://doi.org/10.5194/gmd-2019-5

Geosci. Model Dev. Discuss., https://doi.org/10.5194/gmd-2019-5
Manuscript under review for journal Geosci. Model Dev.
Discussion started: 5 February 2019

Geoscientific Model Development Discussions

A Lagrangian convective transport scheme including a simulation of the time air parcels spend in updrafts

Ingo Wohltmann[1], Ralph Lehmann[1], Georg A. Gottwald[2], Karsten Peters[3,*], Alain Protat[4], Valentin Louf[5], Christopher Williams[6], Wuhu Feng[7], and Markus Rex[1]

[1]Alfred Wegener Institute for Polar and Marine Research, Potsdam, Germany
[2]School of Mathematics and Statistics, University of Sydney, New South Wales, Australia
[3]Max Planck Institute for Meteorology, Hamburg, Germany
[4]Bureau of Meteorology, Melbourne, Australia
[5]Monash University, Clayton, Australia
[6]NOAA, Boulder, Colorado, USA
[7]National Centre for Atmospheric Science, School of Earth and Environment, University of Leeds, Leeds LS2 9JT, UK
[*]now at Deutsches Klimarechenzentrum GmbH (DKRZ), Hamburg, Germany

Correspondence: I. Wohltmann (ingo.wohltmann@awi.de)

Abstract. We present a Lagrangian convective transport scheme developed for Chemistry and Transport Models and ensemble trajectory simulations. Similar to existing schemes in other Lagrangian models, it is based on a statistical approach of calculating parcel displacements by convection. These schemes redistribute air parcels within a fixed time step by calculating probabilities for entrainment and the altitude of detrainment. Our scheme extends this approach by modelling vertical updraft velocities and the time that an air parcel spends inside the convective event, which is important for simulating the tropospheric chemistry of short-lived species, e.g. it determines the time available for heterogeneous processes on the surface of cloud droplets. Two different schemes for determining the vertical updraft velocities are introduced, which are based on constant or random convective area fraction profiles, respectively. SO_2 is used as an example to show that there is a significant effect on species mixing ratios when modelling the time spent in convective updrafts compared to a nearly instantaneous redistribution of air parcels. The scheme is driven by convective mass fluxes and detrainment rates that originate from an external convective parameterization, which can be obtained from meteorological analysis data or General Circulation Models. Validation runs driven by ECMWF ERA Interim reanalysis data are performed with the scheme implemented into the ATLAS Chemistry and Transport Model. These include long-term global trajectory simulations of Radon-222 that are compared to measurements, and runs testing mass conservation and the reproduction of the convective mass fluxes and detrainment rates of ERA Interim. Simulated vertical updraft velocities are validated by wind profiler measurements in Darwin.

1 Introduction

The parameterization of sub-grid scale cumulus convection and the associated vertical transport is not only a key process in General Circulation Models (e.g. Arakawa, 2004), but the correct simulation of convective transport is also important for the

Geosci. Model Dev. Discuss., https://doi.org/10.5194/gmd-2019-5
Manuscript under review for journal Geosci. Model Dev.
Discussion started: 5 February 2019

modelling of tracers in Chemistry and Transport Models, and the treatment of convection is a large source of uncertainty for the simulation of species in the troposphere (e.g. Mahowald et al., 1995; Hoyle et al., 2011; Feng et al., 2011).

We present a Lagrangian convective transport scheme developed for Chemistry and Transport Models and ensemble trajectory simulations. Our convective transport scheme is based on a statistical approach similar to the schemes in other Lagrangian models (e.g. Collins et al., 2002; Forster et al., 2007; Rossi et al., 2016). These schemes redistribute air parcels vertically within a fixed time step to simulate the effect of convection and are driven by convective mass fluxes and detrainment rates derived from a physical parameterization of convection.

However, these schemes do not take into account the different residence times of air parcels inside the convective cloud. The amount of time spent inside the cloud is important for calculations of the tropospheric chemistry of short-lived species. The concentrations of these species in the upper troposphere may crucially depend on the transport time of an air parcel from the boundary layer to the upper troposphere (e.g. Hoyle et al., 2011). Therefore, we extend the approach of earlier schemes by simulating the time air parcels spend inside a convective cloud. An example for a species for which that is relevant is the short-lived species SO_2, which is depleted by a range of fast heterogenous reactions inside clouds and by a gas-phase reaction with OH (e.g. Berglen et al., 2004; Tsai et al., 2010). We perform runs with an artificial tracer that is designed to imitate the most important characteristics of SO_2 chemistry to show that there is a significant effect on tracer mixing ratios when using our scheme compared to a scheme with a nearly instantaneous redistribution.

The scheme is implemented into the ATLAS Chemistry and Transport Model (e.g. Wohltmann and Rex, 2009) and runs driven by ECMWF ERA Interim reanalysis data (Dee et al., 2011) are performed. Section 2 and Section 3 describe the convective transport scheme and the corresponding algorithm. Section 2 describes the modelling of entrainment, upward transport, detrainment and subsidence. Section 3 describes the method to calculate vertical updraft velocities. In Section 4, the scheme is validated. Mass conservation and reproduction of the mass fluxes and detrainment rates from meteorological data are tested, global trajectory based simulations of Radon-222 are compared to measurements, and simulated vertical updraft velocities are compared statistically with wind profiler measurements from Darwin, Australia. In Section 5, simulations with a SO_2-like tracer are shown to demonstrate that using the scheme can have a significant effect on tracer mixing ratios. Section 6 contains the conclusions.

2 Description of the convective transport scheme

2.1 General concept

First, we will present the algorithm for forward trajectories, and will introduce the necessary adaptions for backward trajectories at the end to facilitate understanding.

A statistical approach is taken, where entrainment and detrainment probabilities are calculated for each trajectory at every time step. Whether a given trajectory is entrained into the cloud or detrained from the cloud is then determined by drawing random numbers. The model is driven by convective mass fluxes and detrainment rates from meteorological data or General

Geosci. Model Dev. Discuss., https://doi.org/10.5194/gmd-2019-5
Manuscript under review for journal Geosci. Model Dev.
Discussion started: 5 February 2019

Geoscientific Model Development Discussions

Circulation Models and thus relies on an external convective parameterization. Since a grid box of the meteorological analysis typically contains several convective systems that only cover a small fraction of the grid box, a statistical approach is necessary.

The approach used in existing convective transport schemes is extended here by simulating the time that an air parcel spends inside the convective event. For this, vertical updraft velocities are calculated from the meteorological analysis and some additional assumptions (a detailed account is given in Section 3). Instead of calculating the probability that an entrained air parcel detrains at a certain altitude and then redistributing the parcels in a fixed time step (as in the conventional approach), a trajectory time step is divided into smaller intermediate time steps, and the parcel is moved upwards and tested for detrainment in each intermediate time step.

Our algorithm executes the following steps for each trajectory air parcel in every trajectory time step Δt (typically 10 minutes):

1. Entrainment if air parcel is not in convection and if a test for entrainment is successful (Section 2.2)
2. If the air parcel is in convection, the following two steps are repeated with a smaller convective time step Δt_c of 10 seconds until the air parcel detrains or the end of the present trajectory time step (Δt) is reached:
   - Upward transport by the distance given by the convective time step and the vertical updraft velocity (Section 2.3)
   - Detrainment if a test for detrainment is successful (Section 2.4)
3. Subsidence of air parcels outside of convection in the environment (Section 2.5)

The trajectory time step needs to be sufficiently short for the algorithm to work (see Sections 2.2 and 2.4).

The convective mass flux $M(z)$ at a given location, geometric altitude z and time in units of mass transported per area and per time interval is related to the entrainment rate $E(z)$ and the detrainment rate $D(z)$ by mass conservation

$$\frac{\mathrm{d}M}{\mathrm{d}z} = E - D \tag{1}$$

where E and D are given in units of mass per area, per time interval and per vertical distance. We define both E and D as positive numbers.

In the meteorological data, the atmosphere is divided into several model layers. Usually, the convective mass flux is given at the layer interfaces, while the detrainment rates are given as mean values per layer. Entrainment rates can be calculated from the mass fluxes and detrainment rates by Equation 1. In addition, the atmosphere is divided into grid boxes with a given horizontal resolution in the meteorological analysis. In the ERA Interim meteorological analysis, M is given as the grid box mean convective updraft mass flux and D as the grid box mean updraft detrainment rate per geometric altitude. M is related to the mean convective mass flux in the convective updrafts M_u (per area of updraft) by

$$M = f_u M_u \tag{2}$$

where f_u is the convective area fraction, which is the fraction of the area of the grid box covered by updrafts in convective clouds. We will only consider updrafts here, since updraft mass fluxes typically dominate over downdraft mass fluxes (see e.g. Figure 3 in Kumar et al., 2015). It is planned to simulate downdraft mass fluxes in a future version of the model.

Geosci. Model Dev. Discuss., https://doi.org/10.5194/gmd-2019-5
Manuscript under review for journal Geosci. Model Dev.
Discussion started: 5 February 2019

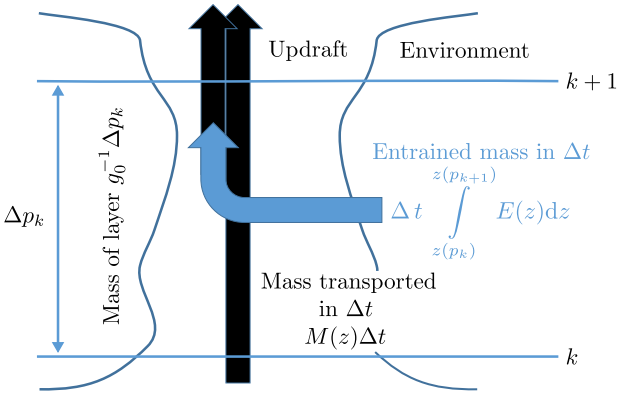

Figure 1. Schematic representation of the entrainment step. All quantities per area.

In the following, it is assumed that the mass associated with a trajectory is equal to the mass of the other trajectories and remains constant. This implies that for global model runs, the trajectories need to be distributed uniformly over pressure. The mass associated with the trajectory is then given by air density at the trajectory location and the volume it occupies. The mass of a trajectory air parcel in such a model is typically much larger than the mass transported in a single convective event (e.g. Collins et al., 2002). For this reason and due to the statistical nature of the approach, results will only be meaningful if a sufficiently large ensemble of trajectories is examined before interpretating the results. The equations of the scheme are independent of the mass associated with the trajectory. Thus, in a global model where the trajectories fill the model domain, a larger mass associated with a trajectory parcel (i.e. a lower density of trajectories per volume) leads to a lower number of trajectories in convection at a given point in time, which balances the higher mass moved per convective event.

2.2 Entrainment

For modelling the entrainment of the trajectories, we assume that the atmosphere is divided in several layers, where layer k is confined by levels k and $k+1$, see Figure 1. These may be identified with the model layers of the meteorological analysis. For an air parcel located in a layer between pressures p_k and p_{k+1}, the probability ε of it being entrained in a trajectory time step Δt is given by

$$\varepsilon = \frac{g_0 \Delta t \int_{z(p_k)}^{z(p_{k+1})} E\,\mathrm{d}z}{\Delta p_k} \quad \text{with} \quad \Delta p_k = p_k - p_{k+1} \tag{3}$$

where g_0 is the gravitational acceleration of the Earth and $\int E\,\mathrm{d}z$ is the grid-box mean entrainment rate integrated over the layer (resulting in the same units as the convective mass flux). The integration has to be performed over geometric altitude, which requires a conversion between pressure and geometric altitude. The equation is derived by dividing the mass per area entrained in a layer in a time step Δt by the mass per area of the layer. It is independent of the area covered by convection.

Whether an air parcel is entrained and takes part in convection is decided by generating a uniformly distributed random number r_e in the interval $[0,1]$ in every trajectory time step and comparing that to the calculated probability. If the random

Geosci. Model Dev. Discuss., https://doi.org/10.5194/gmd-2019-5
Manuscript under review for journal Geosci. Model Dev.
Discussion started: 5 February 2019

Geoscientific Model Development Discussions

number is smaller than the entrainment probability $r_e < \varepsilon$, the air parcel is marked as taking part in convection and is therefore not tested for being entrained as long as it stays in convection. The trajectory time step needs to be sufficiently short for the algorithm to work to avoid that $\varepsilon > 1$ (which would mean that the air in the layer would be ventilated several times by convection during the time step).

The time when the convective event starts can be anywhere in the time interval between t and $t + \Delta t$. For simplicity, we assume that the convective event always starts at time t. This only results in a small shift of the convective event by a few minutes at most (depending on the model time step), which will be negligible in most cases.

2.3 Upward transport

If a parcel is marked as taking part in convection, it is transported upwards for the vertical distance that it will be able to ascend according to the vertical convective updraft velocity in one intermediate convective time step Δt_c (10 seconds). Then, it will be tested for detrainment (see Section 2.4). This procedure will be repeated until either the test for detrainment is successful or the end of the present trajectory time step $t + \Delta t$ is reached. The short intermediate time step is necessary to capture the steep vertical gradients in the detrainment rates and convective mass fluxes. For a strong updraft of $10\,\mathrm{m/s}$, a time step of $10\,\mathrm{s}$ corresponds to a vertical distance of $100\,\mathrm{m}$, which is usually sufficient to resolve the vertical levels of the analyses.

The vertical updraft velocity inside the convective cloud is given by

$$w_u = \frac{MRT}{f_u p} \tag{4}$$

where $R = 287\,\mathrm{J/kg/K}$ is the specific gas constant of air, T is temperature and the quantities are interpolated to the position of the air parcel. The equation is derived by noting that the convective mass flux in the cloud is the product of density and the vertical updraft velocity $M_u = \rho w_u$ (with $\rho = p/(RT)$ according to the ideal gas law), and by using Equation 2. The resulting velocity is in units of geometric altitude per time.

Neither convective area fractions f_u nor vertical updraft velocities w_u are usually available from meteorological analysis data. The approach used to overcome this problem in our convection scheme is to estimate a profile of f_u based on observations. We implement two methods here. The first method uses a constant climatological convective area fraction, while the second uses a stochastic parameterization (Gottwald et al., 2016). A detailed discussion of the calculation of the vertical updraft velocities is given in Section 3.

The vertical geometric distance Δz_{conv} that the air parcel ascends in an intermediate time step is

$$\Delta z_{\mathrm{conv}} = w_u \Delta t_c \tag{5}$$

Under the assumption that the coordinate system of the trajectory model is log-pressure height Z, the distance that the parcel ascends in log-pressure height is

$$\Delta Z_{\mathrm{conv}} = \Delta z_{\mathrm{conv}} \frac{T_0}{T} \tag{6}$$

Geosci. Model Dev. Discuss., https://doi.org/10.5194/gmd-2019-5
Manuscript under review for journal Geosci. Model Dev.
Discussion started: 5 February 2019

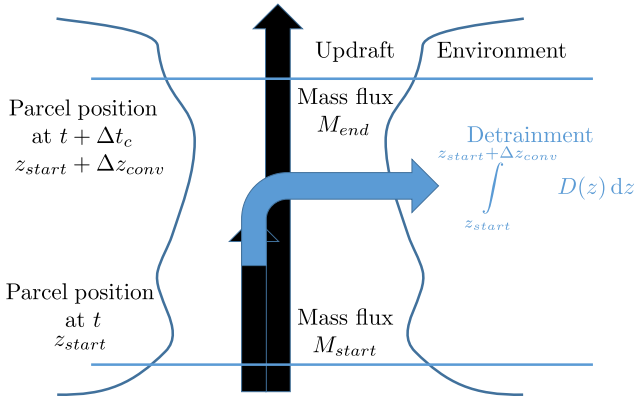

Figure 2. Schematic representation of the detrainment step.

where log-pressure height is defined as $Z = -H \log(p/p_0)$ and $H = RT_0/g_0$. T_0 and p_0 are the reference temperature and reference pressure of the log-pressure coordinate. Other coordinate systems will require equivalent transformations. ΔZ_{conv} is added to the vertical position of the parcel. Longitude and latitude are left unchanged.

2.4 Detrainment

If a parcel is marked as taking part in convection and has been transported upwards, it is tested next for detrainment.

The probability that a parcel is detrained during an intermediate convective time step is

$$\delta = \frac{\int_{z_{\text{start}}}^{z_{\text{start}}+\Delta z_{\text{conv}}} D\,\mathrm{d}z}{M_{\text{start}} + \int_{z_{\text{start}}}^{z_{\text{start}}+\Delta z_{\text{conv}}} E\,\mathrm{d}z} \tag{7}$$

or, equivalently

$$\delta = \frac{\int_{z_{\text{start}}}^{z_{\text{start}}+\Delta z_{\text{conv}}} D\,\mathrm{d}z}{M_{\text{end}} + \int_{z_{\text{start}}}^{z_{\text{start}}+\Delta z_{\text{conv}}} D\,\mathrm{d}z} \tag{8}$$

where M_{start} is the convective mass flux at the start position of the air parcel and z_{start} is the altitude of the start position. $z_{\text{start}} + \Delta z_{\text{conv}}$ is the end position of the air parcel after one intermediate time step (see Figure 2). Conversions from the coordinate system of the trajectory model to geometric altitude are necessary here. The equation is derived by noting that all the air involved in convection in the layer defined by Δz_{conv} (regardless whether it was entrained in that layer or coming from below) can only leave via two paths: either it can be detrained or it can leave through the upper boundary. Thus, the probability is the ratio of the amount of air that is detrained between the start and end position of the air parcel and the sum of the amount of air entering either from below (M_{start}) or through entrainment between the start and end position. The equation assumes that air coming from below behaves the same way as air entrained. That is, there is no preferred pathway out of the layer for air coming from below or for air entrained.

Geosci. Model Dev. Discuss., https://doi.org/10.5194/gmd-2019-5
Manuscript under review for journal Geosci. Model Dev.
Discussion started: 5 February 2019

Geoscientific Model Development Discussions

Next, another uniformly distributed random number r_d is generated. If the random number is smaller than the detrainment probability $r_d < \delta$, the parcel leaves the convection at altitude

$$z_{\text{detrain}} = z_{\text{start}} + \Delta z_{\text{conv}} \frac{r_d}{\delta} \tag{9}$$

Multiplication with r_d/δ ensures that the detrainment heights are uniformly distributed in $[z_{\text{start}}, z_{\text{start}} + \Delta z_{\text{conv}}]$. This is more realistic than assuming that the air parcel always leaves at $z_{\text{start}} + \Delta z_{\text{conv}}$. This would overestimate the detrainment altitude systematically, since δ is the probability that the parcel detrains somewhere between z_{start} and $z_{\text{start}} + \Delta z_{\text{conv}}$. A parcel can entrain and detrain in the same trajetory time step Δt (but can stay longer in convection, of course).

If the parcel reaches an altitude where the convective mass flux M interpolated to the position of the parcel is zero, but still has not detrained, the parcel is forced to detrain. Due to the finite time step, the air parcel may end up at a position where $M = 0$, which can be interpretated as numerical overshooting. While this behaviour can be avoided by decreasing the altitude of the parcel until $M > 0$, we choose not to correct for this.

If the air parcel detrains before reaching the end of the present trajectory time step, it cannot entrain again until the start of the next time step. A correction can be applied to account for the missing simulated time between the detrainment event (which is at some intermediate time step) and the start of the next trajectory time step. This can be accomplished by adding the missing time to the Δt of the next entrainment test of the trajectory. The effect of this correction is usually small, if the trajectory time step is not chosen to large. Since the trajectory model output is only on the regular grid of the trajectory time steps, the trajectory is marked as detraining only at the time of the next trajectory time step and not at the intermediate time step. If the trajectory time step is too large, this can have an effect on both the distribution of the residence times in convection (see Figure 14) and on the chemistry of short-lived species (see discussion of SO_2-like tracer in Section 5).

2.5 Subsidence outside of convective systems

To conserve mass and balance the updraft, parcels in the environmental air have to subside. All parcels that are currently not in convection are moved downwards by a pressure difference of

$$\Delta p_{\text{subsidence}} = \frac{1}{1 - f_u} g_0 M \Delta t \tag{10}$$

where M and f_u are the convective mass flux and convective area fraction interpolated to the position of the trajectory parcel. The factor $1/(1 - f_u)$ is a weight introduced to compensate for not subsiding the trajectory air parcels that are in convection, but is close to unity since f_u is small. The fraction of trajectories that are in convection will not necessarily correlate to f_u, which is based on observations independent from the convective parameterization.

2.6 Backward trajectories

A nice property of the algorithm is that it also works for backward trajectories. Backward trajectories with convection are e.g. useful for determining the source regions and modelling the chemical composition of air measured along a flight path or sonde ascent.

Geosci. Model Dev. Discuss., https://doi.org/10.5194/gmd-2019-5
Manuscript under review for journal Geosci. Model Dev.
Discussion started: 5 February 2019

Some modifications of the algorithm are necessary. First, we have to exchange the meaning of E and D in the equations (detrainment becomes entrainment backwards in time). Then, the updraft velocity w_u has a negative sign. Finally, the correction for subsidence moves the air parcels upward. The "entrainment" probabilities from Equation 3 (actually "detrainment probabilities backwards in time") become

$$\varepsilon = \frac{g_0 \Delta t \int_{z(p_k)}^{z(p_{k+1})} D \, \mathrm{d}z}{\Delta p_k} \quad \text{with} \quad \Delta p_k = p_k - p_{k+1} \tag{11}$$

The "detrainment" probabilities become

$$\delta = \frac{\int_{z_\mathrm{start} - \Delta z_\mathrm{conv}}^{z_\mathrm{start}} E \, \mathrm{d}z}{M_\mathrm{start} + \int_{z_\mathrm{start} - \Delta z_\mathrm{conv}}^{z_\mathrm{start}} D \, \mathrm{d}z} \tag{12}$$

In contrast to forward trajectories, the convective mass flux at the start position of the air parcel M_start is at a higher altitude z_start than the end position $z_\mathrm{start} - \Delta z_\mathrm{conv}$.

If the parcel reaches either an altitude where $M = 0$ or goes below the surface (due to the finite time step), but still has not "detrained" the parcel is forced to "detrain".

3 Simulation of vertical updraft velocities

Vertical updraft velocities can be calculated by Equation 4, where most quantities can be obtained from the meteorological analysis data. However, the convective area fraction f_u is not available from the meteorological analysis and has to be obtained independently.

3.1 Constant convective area fraction

The first method is to use a constant climatological profile $f_u(z)$ of the convective area fraction. For this profile, we use C-band dual polarization (CPOL) radar measurements conducted in Darwin, Australia, and define a profile which closely follows the profile in Figure 2 of Kumar et al. (2015) (red lines using the "space approach"). The profile is representative for a 190 x 190 km^2 grid box centered over Darwin and is shown in Figure 3. As a result, the variability of the vertical velocities arises mainly from the variability of M then. The choice of a tropical profile is affected by our first application cases. An obvious shortcoming of this method is that it assumes a globally constant convective area fraction, which is certainly not realistic. Hence, we implement a second method to improve on this.

3.2 Random convective area fraction

The second method uses a stochastic parameterization of the convective area fraction conditioned on the large scale vertical velocity at 500 hPa, which is described by Gottwald et al. (2016). The method is based on estimates of convective area fractions derived from CPOL radar measurements over Darwin (wet seasons 2004/2005, 2005/2006, 2006/2007, Davies et al., 2013) and Kwajalein, Marshall Islands (May 2008 to January 2009) averaged over 6 hours. The large-scale meteorological state, e.g. the

Geosci. Model Dev. Discuss., https://doi.org/10.5194/gmd-2019-5
Manuscript under review for journal Geosci. Model Dev.
Discussion started: 5 February 2019

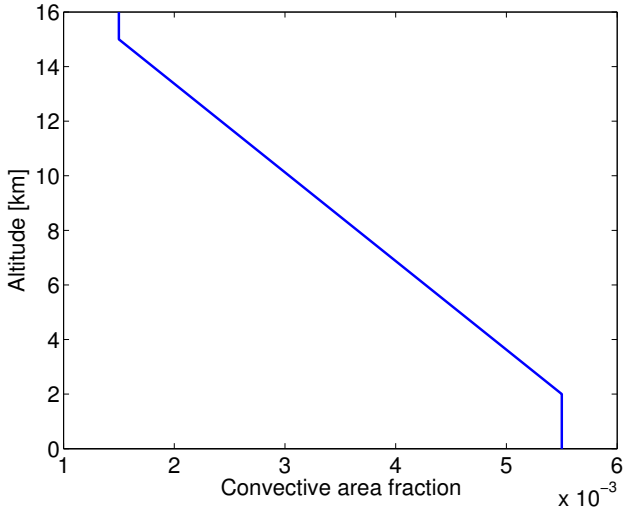

Figure 3. Constant convective area fraction profile used for calculating vertical updraft velocities.

500hPa vertical velocity, was derived by Davies et al. (2013) using a variational analysis. Frequency distributions are derived from the measurements as a function of the large scale vertical velocity at 500 hPa, see Figs. 1 a and b of Gottwald et al. (2016).

Here, we combine the Darwin and Kwajalein data into one data set to increase the number of measurements. Peters et al. (2013) and Gottwald et al. (2016) have shown that the functional dependency of convection on the large-scale meteorological state is sufficiently similar between both locations.

For deriving the frequency distribution, data are binned into a 2-dimensional lookup table, which uses bins for the large scale vertical velocity and bins for the natural logarithm of convective area fraction. The logarithm is used to obtain a more even distribution over the bins. The data are binned in 0.005 $\mathrm{m/s}$ (1.2 $\mathrm{hPa/h}$) bins from -0.035 $\mathrm{m/s}$ to 0.04 $\mathrm{m/s}$ for the large scale vertical velocity and in 0.5 bins from -12 to -2 for the logarithm of the convective area fraction. For values of the large-scale vertical velocity greater than 0.04 $\mathrm{m/s}$ (smaller than -10.2 $\mathrm{hPa/h}$), we use a deterministic relationship obtained by linear regression, since there is not sufficient data for these values of the large-scale vertical velocity.

The large scale vertical velocity of ERA Interim at 500 hPa interpolated to the position of the trajectory is used to select one of the vertical velocity bins of the frequency distribution. Next, a uniformly distributed random number is drawn to determine a value for the convective area fraction from the lookup table.

This value is used as the convective area fraction at cloud base. To obtain a vertical profile, the value is then scaled with a normalized version of the profile from Kumar et al. (2015) from the first method. Then, vertical updraft velocities can be calculated from Equation 4. The scaling with a constant profile ensures that the resulting profile of vertical updraft velocities will be physically reasonable (in contrast to a method where the vertical updraft velocity would be obtained independently at every level). Ideally, we would like to draw the convective area fraction at all levels stochastically conditioned on the vertical

velocities at all levels. The limited amount of observational data available, however, does not allow for this more involved parametrization.

Due to the random character of the method, it is unavoidable that unrealistic vertical updraft velocities are produced from time to time. This may also be caused by the fact that the method to obtain f_u does not take into account the value of the convective mass flux at the trajectory position. Hence, values above $20\,\mathrm{m/s}$ are reset to $20\,\mathrm{m/s}$. Values below $0.1\,\mathrm{m/s}$ are reset to $0.1\,\mathrm{m/s}$ to avoid that the trajectories remain in convection for too long. This only affects at most a few percent of the trajectories.

3.3 Limitations and possible alternatives

An alternative approach is to use a climatological profile of measured mean vertical velocities together with some method to obtain variability by scaling the profile, i.e. not to use Equation 4. However, this has the disadvantage that the shape of the wind profile is always the same. Measurements of updraft velocities are available from in situ aircraft observations (e.g. LeMone and Zipser, 1980), airborne Doppler radar (e.g. Heymsfield et al., 2010) or ground-based wind profilers (e.g. May and Rajopadhyaya, 1999; Kumar et al., 2015). In combination with the given convective mass fluxes, this method of obtaining the vertical updraft velocities may lead to inferred convective area fractions greater than 1. This issue is equivalent to the issue of the unrealistic vertical updraft velocities in the method using the convective area fractions.

A limitation of our method to derive f_u is that it does not take into account the convective mass flux at the trajectory position. It may be possible to base the convective area fractions on convective mass flux as the large scale variable. This requires measured convective mass fluxes, which can only be obtained from simultaneous measurements of convective area fractions and updraft velocities (see Kumar et al., 2015).

4 Validation of the convective transport scheme

For validation of the convective transport scheme, we perform trajectory simulations driven by meteorological data of the ECMWF ERA Interim reanalysis (Dee et al., 2011) with 2° x 2° horizontal resolution, which include large scale wind fields, temperature, updraft convective mass fluxes, detrainment rates and boundary layer heights. Large scale winds and temperatures are used with $6\,\mathrm{h}$ temporal resolution, while convective mass fluxes, detrainment rates and boundary layer heights are used with $3\,\mathrm{h}$ resolution to capture the diurnal cycle. Entrainment rates are not provided by ECMWF and are calculated from the detrainment rates and convective mass fluxes. The convective parameterization of the ERA Interim reanalysis in the underlying IFS model is originally based on the scheme of Tiedtke (1989), with several modifications (e.g. Bechtold et al., 2004). The trajectory model is the model that is used in the ATLAS Chemistry and Transport Model (Wohltmann and Rex, 2009), extended for the convective transport scheme.

While the quality of the used convective mass fluxes and detrainment rates will have a large impact on the results of the Radon validation and the validation of the vertical updraft velocities, it is out of the scope of this study to give a validation of ERA Interim. We refer the reader to the existing literature here (e.g. Dee et al., 2011; Taszarek et al., 2018).

Geosci. Model Dev. Discuss., https://doi.org/10.5194/gmd-2019-5
Manuscript under review for journal Geosci. Model Dev.
Discussion started: 5 February 2019

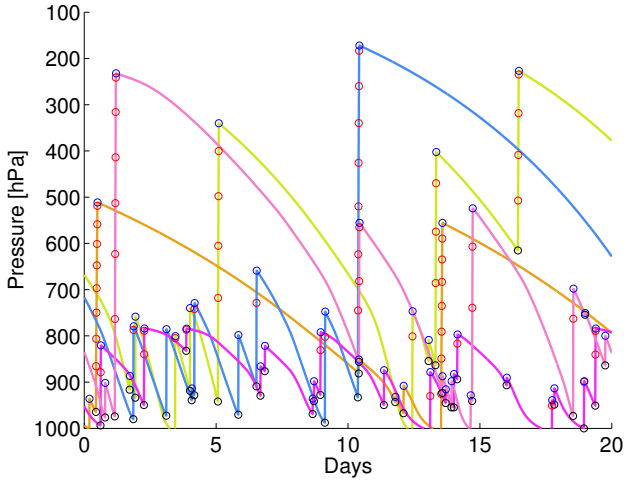

Figure 4. Example trajectories from the run with the simplified setup with large scale wind set to zero for forward trajectories and constant convective area profile. Open black circles mark entrainment, open red circles upward transport in convection in 10 minute steps and open blue circles detrainment.

4.1 Mass conservation and reproduction of convective mass fluxes and detrainment rates

For the technical verification of the algorithm, we test mass conservation and the reproduction of the archived convective mass fluxes and detrainment rates. We use a simplified and non-realistic setup here that facilitates interpretation. How well the results of our model compare with reality is an independent issue that will be discussed in Section 4.2 and is examined with a more realistic setup. We also use the more realistic setup to test mass conservation more rigorously later.

In the simplified setup, we start 100,000 trajectories that are uniformly distributed in pressure between 1000 hPa and 100 hPa and uniformly distributed horizontally between 180° E and 240° E and 30° S and 30° N (Pacific Ocean). The horizontal domain is chosen due to the flat orography and since the first applications of our model will be in the tropics. The runs are driven by temporally constant convective mass fluxes and detrainment rates from ERA Interim taken from the arbitrary date 1 June 2010, 00 h UTC. Large-scale horizontal and vertical winds are set to zero. I.e., trajectories can only move vertically by convection and subsidence. Trajectories that travel below the surface due to the finite time step are lifted above the surface again. Trajectories are run for 20 days, the trajectory time step is 10 minutes and the trajectory model uses a log-pressure coordinate. Four different runs are performed for forward and backward trajectories and for the two vertical updraft velocity parameterizations (see Sections 3.1 and 3.2). Each trajectory is assigned a constant mass given by the volume it occupies. Figure 4 shows some arbitrarily selected trajectories from the forward run with the constant convective area fraction profile (Section 3.1) as examples.

Figure 5 shows the mass conservation for forward trajectories and the constant convective area fraction profile. The number of the trajectories in 50 hPa bins at the start of the run (blue) compares well to the number of trajectories in these bins at the end of the run (red). There is only a small deviation at the lowest levels caused by the fact that all trajectories are initialized

Geosci. Model Dev. Discuss., https://doi.org/10.5194/gmd-2019-5
Manuscript under review for journal Geosci. Model Dev.
Discussion started: 5 February 2019

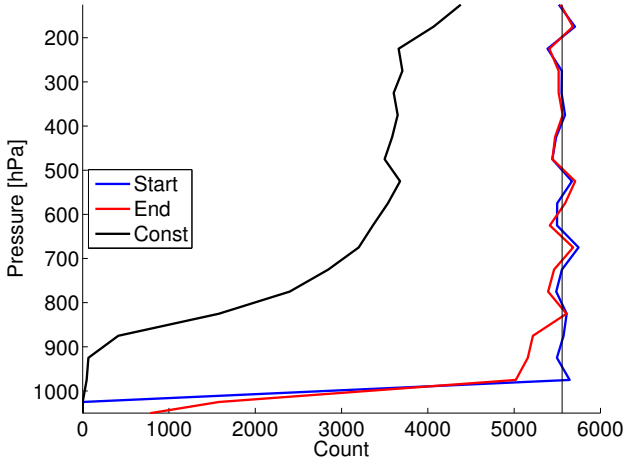

Figure 5. Mass conservation after 20 days for forward trajectories and using a constant convective area fraction profile. Number of trajectories in 50 hPa bins at the start of the run (blue) and at the end of the run (red). The black line denotes the number of trajectories that did not move due to zero convective mass flux at their start position.

with pressures lower than 1000 hPa, but that some surface pressures from ERA Interim in the simulated region are higher. This causes some trajectories to end with pressures above 1000 hPa. Results for backward trajectories or the random convective area fraction profile look very similar (not shown).

In the simplified setup, a significant fraction of the trajectories will not move at all, because they are initialized in a position where the convective mass flux and entrainment rate are zero. In Figure 5, the number of these trajectories is shown in black. A more rigorous test of mass conservation with a long-term simulation driven by the actual large scale wind fields is shown in the next section.

Figure 6 shows the mean convective mass flux profile from ERA Interim averaged over the tropical domain described above compared with the simulated mass flux profile for forward trajectories and with the constant convective area fraction profile. Simulated mass fluxes are calculated by counting the trajectories that pass a given pressure level during one trajectory time step and which are in convection at this time. The number of the trajectories is multiplied with the trajectory mass then and divided by the area of the tropical domain and the time period of 20 days. The agreement between ERA Interim and the simulations is very good. There is only a slight underestimation of the pronounced maximum around 950 hPa. Results for backward trajectories or random convective area fraction profiles look very similar (not shown).

Figure 7 shows the same for the detrainment rates. Detrainment rates are calculated by counting the trajectories that have a detrainment event in a given pressure layer during one trajectory time step. The number of the trajectories is multiplied with the trajectory mass, divided by the area of the tropical domain, the time period of 20 days and the mean vertical extent in geometrical altitude of the pressure layer. Again, agreement is very good and results for backward trajectories or random convective area fraction profiles look very similar (not shown).

Geosci. Model Dev. Discuss., https://doi.org/10.5194/gmd-2019-5
Manuscript under review for journal Geosci. Model Dev.
Discussion started: 5 February 2019

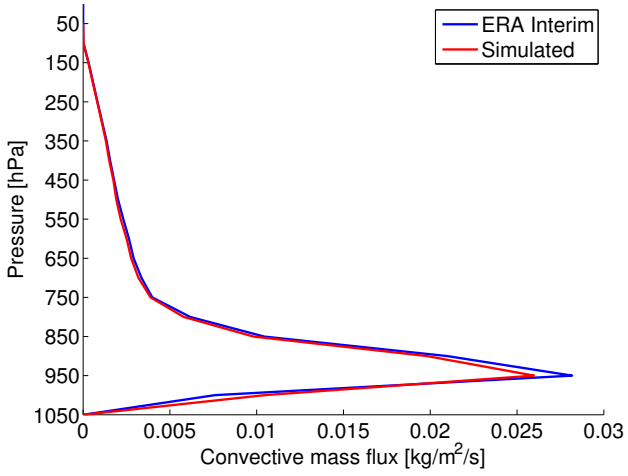

Figure 6. Mean convective mass flux profile from ERA Interim compared to the simulated convective mass flux profile for forward trajectories and using a constant convective area fraction profile (in a region from 180° E to 240° E and 30° S to 30° N, 20 days with meteorological fields of 1 June 2010).

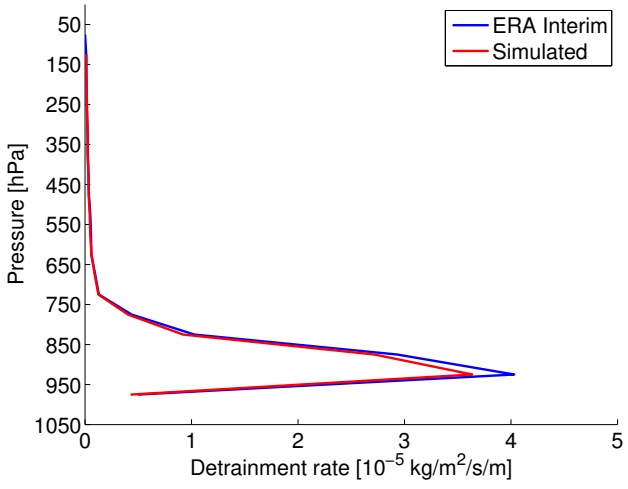

Figure 7. Mean detrainment rate profile from ERA Interim compared to the simulated detrainment rate profile for forward trajectories and constant convective area fraction profile (in a region from 180° E to 240° E and 30° S to 30° N, 20 days with meteorological fields of 1 June 2010).

Geosci. Model Dev. Discuss., https://doi.org/10.5194/gmd-2019-5
Manuscript under review for journal Geosci. Model Dev.
Discussion started: 5 February 2019

4.2 Validation of the convection scheme with Radon-222

A validation with measurement data is performed by comparing the results of long-term global trajectory simulations of Radon-222 to measurements. These results will depend on the used meteorological data.

Radon-222 is formed by the radioactive decay of uranium in rock and soils and has been widely used to validate convection models and to evaluate tracer transport (e.g. Jacob et al., 1997; Feng et al., 2011). Its popularity is due to some favorable properties: It is chemically inert, is not subject to wet and dry deposition and is only removed by radioactive decay. The half-life time of 3.8 days is in the right order of magnitude to detect changes in convective transport. However, the measurement coverage of Radon is quite limited (in particular for profiles) and emissions, which can vary with region and time, are uncertain (e.g. Liu et al., 1984; Mahowald et al., 1995).

Global runs are performed for the time period 1 January 1989 to 31 December 2005. Trajectories are initialized at random positions with 150 km horizontal resolution in layers of 50 hPa from 1100 hPa to 50 hPa. Trajectories initialized below surface are deleted. The trajectory model uses a log-pressure coordinate and is driven by ERA Interim data. The trajectory time step is set to 30 minutes. Trajectories that travel below the surface due to the finite time step are lifted above the surface again. In the uppermost layer (100 hPa to 50 hPa), trajectory positions are reinitialized at random positions in every time step. There is no special treatment of the boundary layer except for the assumption of a well-mixed layer when distributing the Radon emissions. There is also no mixing of air parcels to simulate diffusion, contrary to the stratospheric version of the model (Wohltmann and Rex, 2009). Given the resolution of the model runs and the short half-life time of Radon, we believe that these simplifications are justified.

Figure 8 shows the mass conservation of the long-term simulation. The number of trajectories in 50 hPa bins at the start of a run with convection and the constant convective area fraction profile (cyan) compares very well with the mass distribution at the end of the run (magenta) and the results of a run without convection (blue and red). The lower number of trajectories in the bins near the surface is due to orography. The trajectories remain homogeneously distributed in the horizontal domain without clustering or forming gaps over the course of the model run, and hence no further measures are applied to redistribute trajectories (not shown).

We use the same Radon emissions as in e.g. Jacob et al. (1997) and Feng et al. (2011). The radon emissions are $1.0\,\mathrm{atoms\,cm^{-2}s^{-1}}$ over land between 60° S–60° N, $0.005\,\mathrm{atoms\,cm^{-2}s^{-1}}$ over oceans between 60° S–60° N, $0.005\,\mathrm{atoms\,cm^{-2}s^{-1}}$ between 60° and 70° in both hemispheres and zero polewards of 70°. Radon is emitted into all trajectory air parcels that are in the boundary layer. Boundary layer height is taken from ERA Interim. Radon is distributed evenly over these parcels by assuming a well-mixed boundary layer, which means adding a volume mixing ratio of

$$\frac{e\,\Delta t}{\Delta z_{\mathrm{BL}}}\frac{k_B T}{p} \tag{13}$$

to each air parcel in the boundary layer, where e is the emission in atoms per area and time interval, Δt is the trajectory model time step, $k_B = 1.38 \cdot 10^{-23}\,\mathrm{J/K}$ is the Boltzmann constant and Δz_{BL} is the local height of the boundary layer.

To avoid large horizontal areas without any trajectories that receive Radon emissions, a minimum boundary layer height of 500 m is used. While the factor $1/\Delta z_{\mathrm{BL}}$ would still ensure mass conservation if no minimum boundary layer height is assumed

Geosci. Model Dev. Discuss., https://doi.org/10.5194/gmd-2019-5
Manuscript under review for journal Geosci. Model Dev.
Discussion started: 5 February 2019

(the decreasing number of air parcels in a given area receiving emissions when decreasing the height of the boundary layer is balanced by the increasing concentration in the fewer parcels that receive emissions), emissions would become patchy and the horizontal resolution of the emission fields would not be fully used.

Unfortunately, there is only a limited number of vertical profile measurements of Radon. We compare the simulations to the climatological mid-latitude profiles of Liu et al. (1984), which have been widely used to validate tracer transport in global models in the past (e.g. Collins et al., 2002; Feng et al., 2011). These observations were obtained from aircraft measurements at different continental locations in the northern midlatitudes from 1952 to 1972. Figure 9 shows the mean simulated Radon profile for June to August over land (30° N–60° N) compared to the Liu et al. (1984) mean measurement profile for the same season (from 23 sites, bars show standard deviation of the profiles). Simulations are averaged over all 15 years of the long-term run, but the years are not identical to the years of measurement, since there is no meteorological data from ERA Interim for this time period. Figure 10 shows the same for December to February (7 sites, no standard deviation available).

In addition, we show comparisons to aircraft campaign measurements from coastal locations around Moffett Field (37.5° N, 122° E, California) in June and August 1994 in Figure 11 (Kritz et al., 1998) and to aircraft measurements from coastal regions in Eastern Canada (Nova Scotia) from the North Atlantic Regional Experiment (NARE) campaign in August 1993 in Figure 12 (Zaucker et al., 1996). Simulation results are averaged over the campaign periods and a longitude-latitude bounding box encompassing all aircraft measurements.

The agreement to the measurements is reasonable, given the large uncertainties in measurements and emissions. Runs with convection agree better with the measurements than runs without convection. There is an underestimation of Radon by the simulations in the middle troposphere. This may be caused by the fact that several measurements are from coastal areas, where the Radon gradient is high and difficult to model.

The results for both vertical updraft velocity parameterizations are nearly identical because of the globally constant lifetime of Radon (a globally constant lifetime implies that for an air parcel in a given layer, only the time since the last contact with the boundary layer matters and not the exact path that the trajectory has taken to the layer). For the same reason, an almost instantaneous redistribution of air parcels as in Collins et al. (2002) will also lead to results very similar to the results shown for the two vertical updraft velocity parameterizations. Hence, it is not possible to give a recommendation for one of the vertical updraft velocity parameterizations from the results of the Radon simulations.

For this reason, we perform runs with a SO_2-like tracer with a varying lifetime in Section 5. Unfortunately, species like SO_2, where different vertical updraft velocity parameterizations lead to significantly different tracer concentrations are often difficult to validate with measurements. This is due to the large uncertainties in the chemistry schemes and microphysics for these species, uncertain emissions and sparse measurement coverage.

4.3 Validation of the vertical updraft velocities with wind profiler measurements

Modelled vertical updraft velocities are validated by comparison to wind profiler measurements. The modelled vertical updraft velocities are taken from the simplified forward trajectory run in the tropical Pacific from Section 4.1. Results for backward trajectories are very similar (not shown).

Geosci. Model Dev. Discuss., https://doi.org/10.5194/gmd-2019-5
Manuscript under review for journal Geosci. Model Dev.
Discussion started: 5 February 2019

Geoscientific Model Development Discussions

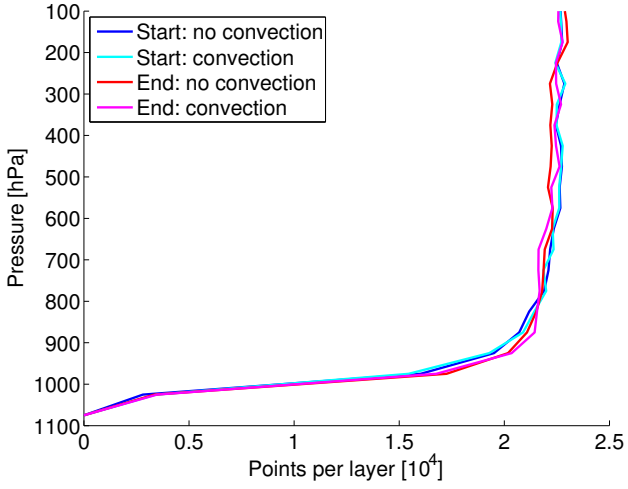

Figure 8. Long term mass conservation after 15 years for a run with forward trajectories and the constant convective area fraction profile, compared to a run without convection. Number of trajectories in 50 hPa bins at the start of the run (blue and cyan) and at the end of the run (red and magenta).

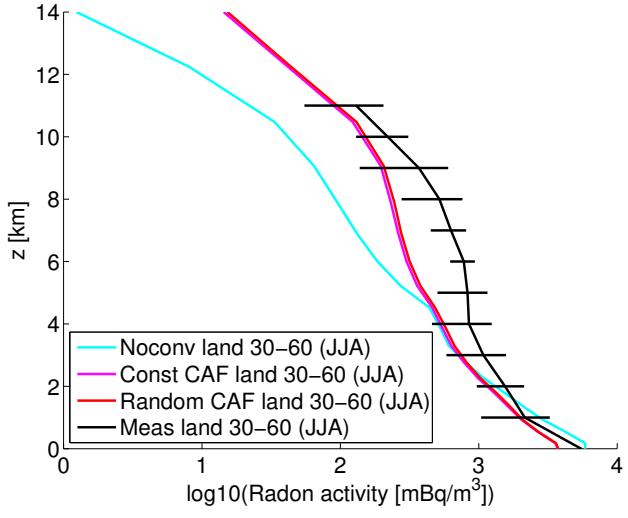

Figure 9. Mean observed radon profile measured over land (30° N–60° N, June–August) from Liu et al. (1984) compared to the simulated Radon from a 15 year long-term run for the same region and months. Bars show the standard deviation of the profiles.

Geosci. Model Dev. Discuss., https://doi.org/10.5194/gmd-2019-5
Manuscript under review for journal Geosci. Model Dev.
Discussion started: 5 February 2019

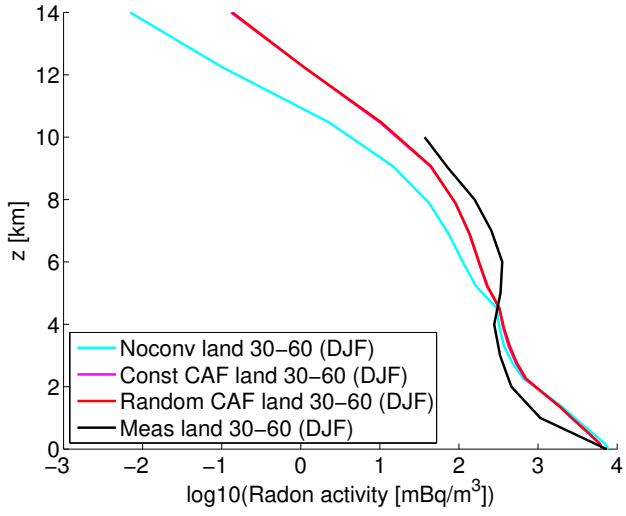

Figure 10. Mean observed radon profile measured over land (30° N–60° N, December–February) from Liu et al. (1984) compared to the simulated Radon from a 15 year long-term run for the same region and months.

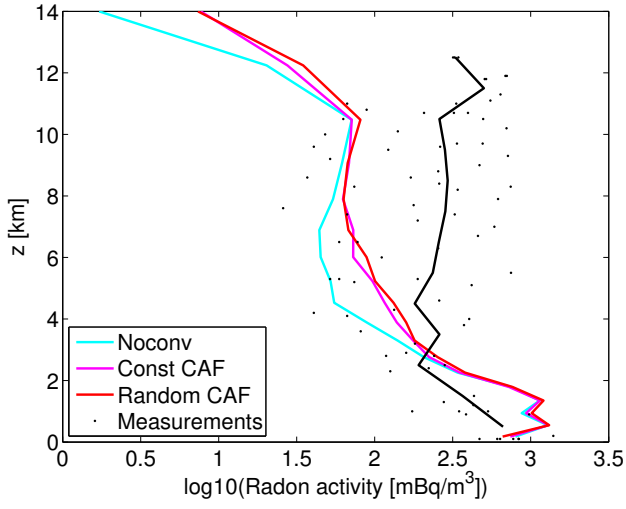

Figure 11. Observed radon from aircraft measurements of the Moffett Field campaign (California) in June 1994 (Kritz et al., 1998) compared to the simulated Radon in the same time period and a bounding box including all measurements. Dots show the single measurements and the solid black line the mean in 1 km bins.

Geosci. Model Dev. Discuss., https://doi.org/10.5194/gmd-2019-5
Manuscript under review for journal Geosci. Model Dev.
Discussion started: 5 February 2019

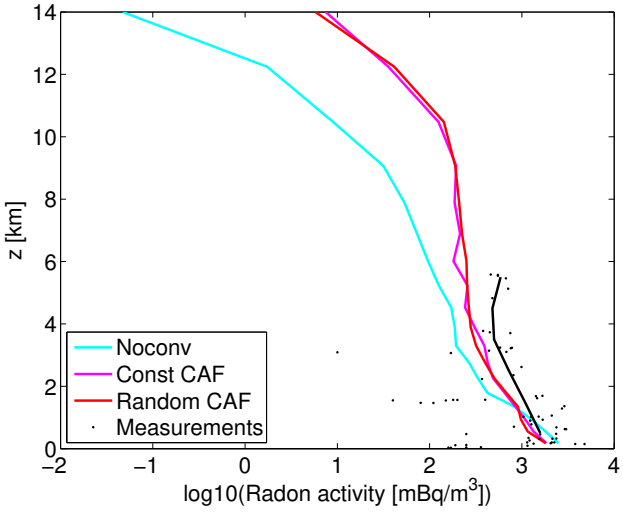

Figure 12. Observed radon from aircraft measurements of the North Atlantic Regional Experiment (NARE) campaign in August 1993 (Zaucker et al., 1996) compared to the simulated Radon in the same time period and a bounding box including all measurements. Dots show the single measurements and the solid black line the mean in 1 km bins.

The modelled velocities are compared statistically with measurements from a 50- and 920-MHz wind profiler pair situated in Darwin, Australia. The time resolution of the measurements is 1 min and vertical updraft velocities are obtained by the method of Williams (2012). Data comprise the wet seasons 2003/2004, 2005/2006, 2006/2007 and 2009/2010. Cloud top heights are determined from the 0 dBz echo top height of the CPOL radar instrument at Darwin. The field of view of this instrument covers the wind profiler site. Convective profiles are identified by using only measurements that show convective precipitation in the CPOL measurements. CPOL data are available every 10 min. All wind profiler measurements within ± 5 min of the CPOL measurement times are considered and cut at the corresponding cloud top height.

Figure 13 shows frequency distributions of the vertical updraft velocities binned in 0.2 m/s bins and for selected 50 hPa pressure bins. Frequency distributions of the vertical updraft velocities from the Darwin measurements are shown in black, modelled distributions from the constant convective area fraction profile method are shown in magenta and modelled distributions from random convective area fraction profile method are shown in red. The solid lines show the distributions with all measurements and all modelled values below 0.6 m/s excluded, while the dashed lines show distributions with all velocity values included.

There is a high number of measurements with small vertical updraft velocities. The sensitivity of the measured distribution to the many small values is quite large, and the measured distributions cut at 0.6 m/s differ significantly from the measured distributions showing all values. The modelled distributions show considerably less values below 0.6 m/s, and the modelled distributions cut at 0.6 m/s agree well with the modelled distributions showing all values.

The agreement between the measurements and the modelled values for the random convective area fraction method is quite satisfactory, when only velocities greater than 0.6 m/s are considered, giving some confidence in the method. In particular, the

Geosci. Model Dev. Discuss., https://doi.org/10.5194/gmd-2019-5
Manuscript under review for journal Geosci. Model Dev.
Discussion started: 5 February 2019

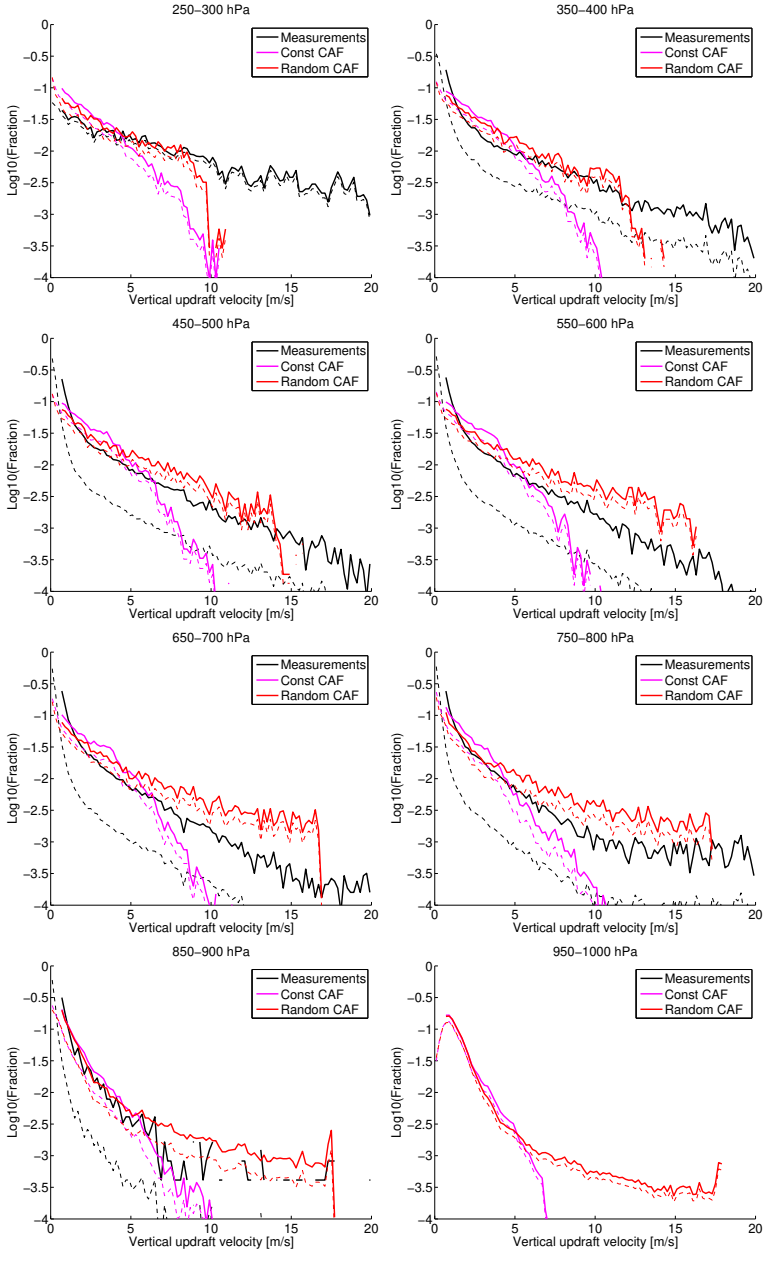

Figure 13. Frequency distribution of vertical updraft velocities for different pressure bins from wind profiler measurements in Darwin, Australia, in 0.2 m/s bins (black), compared to the corresponding frequency distributions of vertical updraft velocities obtained from the constant and random convective area fraction profile method (magenta and red). The dashed lines show the distribution including all velocity values ($> 0\,\mathrm{m/s}$), for the solid lines all values below $0.6\,\mathrm{m/s}$ are excluded.

magnitude of the exponential decrease in the frequency distribution is met quite well. Using the random convective area fraction profile method clearly leads to higher vertical velocities on average than using the constant convective area fraction profile. I.e., the random convective area fraction profile method shows a higher frequency of large vertical velocities than the constant convective area fraction profile method, which is in better agreement with observations. The agreement of the measurements to the modelled values from the constant convective area fraction method is worse for values of more than $5\,\mathrm{m/s}$ than for the random convective area fraction method.

It is difficult to say what the reason for the marked disagreement between model and measurements in the small vertical updraft velocities is. The number of small values is sensitive to the method to determine convective situations in the wind profiler measurements, and may change significantly depending on the method. It is common in other publications to apply a lower threshold to the vertical updraft velocities to obtain convective profiles (e.g. LeMone and Zipser, 1980; May and Rajopadhyaya, 1999; Kumar et al., 2015). For the modelled profiles, the distribution of the velocities is determined by a large number of factors and may change significantly depending on the details of implementation and the convective parameterization in the underlying meteorological analysis. E.g., the assumed convective area fraction profile and the assumptions in the Tiedtke scheme will play a large role. Hence, we don't expect more than a qualitative agreement between model and measurements.

Note that the model is trained on convective area fraction data measured in Darwin and Kwajalein and compared to wind profiler data measured at Darwin, while it is applied to a larger region covering a large part of the tropical Pacific here. The lack of other measurements does not allow for a completely independent model validation.

4.4 Residence time in convection

Figure 14 shows the frequency distribution of the residence times of the trajectories between entrainment and detrainment simulated by the two parameterizations for the vertical updraft velocity (solid lines). It is evident that most convective events have a residence time of less than 30 minutes (more than 95% for the constant convective area fraction profile). Since the number of convective events is dominated by shallow convective events, which typically only lift the air parcel a few $100\,\mathrm{m}$ in one trajectory time step (see Figure 4), we also show the frequency distribution for deep convection (approximated by detrainment events above $300\,\mathrm{hPa}$). These will be more relevant for the upper tropospheric mixing ratio of short-lived species. Typical residence times of deep convective events are around 1 hour for the constant convective area fraction profile. The simulation with the random convective area fraction profile shows a higher number of convective events with a short residence time and correspondingly, a lower number with long residence time, compared to the simulation with constant convective area fraction profile. This is consistent with the larger simulated vertical updraft velocities for the random profile.

5 Simulations with a SO_2-like tracer

To demonstrate that there is a benefit to simulate the vertical updraft velocity and the time spent in convective clouds, we perform runs with an artificial tracer that is designed to imitate the most important characteristics of the short-lived species SO_2 (a detailed model of SO_2 chemistry and emissions is complex and is outside the scope of this study). SO_2 is depleted

Geosci. Model Dev. Discuss., https://doi.org/10.5194/gmd-2019-5
Manuscript under review for journal Geosci. Model Dev.
Discussion started: 5 February 2019

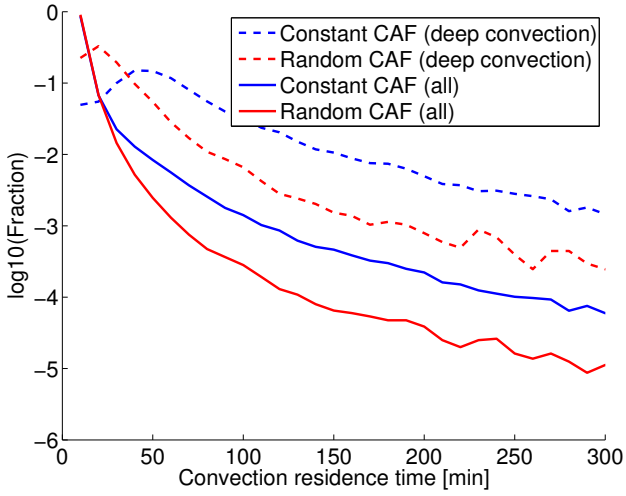

Figure 14. Frequency distribution of the residence times of the trajectories between entrainment and detrainment simulated by the two parameterizations for the vertical updraft velocity. Shown is the fraction of all events with a given duration in 10 minute bins. Solid lines show the distribution for all convective events, while dashed lines show the contribution from deep convective events (detrainment above 300 hPa).

by gas-phase reaction with OH and by several fast heterogenous reactions in the liquid phase in clouds (mainly by H_2O_2). The lifetime with respect to the OH reaction is on the order of days to weeks (e.g. Rex et al., 2014), while the lifetime in the presence of clouds is on the order of hours to days (e.g. Lelieveld, 1993). Hence, we perform runs with a tracer which has a lifetime of 0.1 days when in convection and of 10 days when not in convection. Emissions are distributed uniformly over the globe. Trajectory time step is 10 minutes.

Four different runs are performed: a run without convection, a run with a constant convective area fraction profile, a run with random convective area fraction profiles and a run where the vertical updraft velocity is set to a constant value of 100 m/s to mimic the almost instantaneous redistribution in other Lagrangian convective transport schemes (e.g. Collins et al., 2002). The setup of the runs is identical to the Radon runs, except again that only one year is simulated.

Figure 15 shows the mean simulated profiles in the tropics (30° S–30° N) for the four different runs. The run without convection shows larger values than the other runs in the lower troposphere, since the tracer is always depleted with a long lifetime of 10 days. The runs with convection show smaller values due to the fast depletion in the convective cloud. In the upper troposphere, the run without convection shows lower values than the other runs, since the transport times to the upper troposphere are much longer in the run without convection. In the runs with convection, larger vertical updraft velocities lead to shorter residence times in the cloud, and hence, to higher values of the tracer.

While the difference between the run with the almost instantaneous redistribution and the runs using the convective area fraction is significant, the two schemes for the convective area fraction only show a small difference. This means that the

Geosci. Model Dev. Discuss., https://doi.org/10.5194/gmd-2019-5
Manuscript under review for journal Geosci. Model Dev.
Discussion started: 5 February 2019

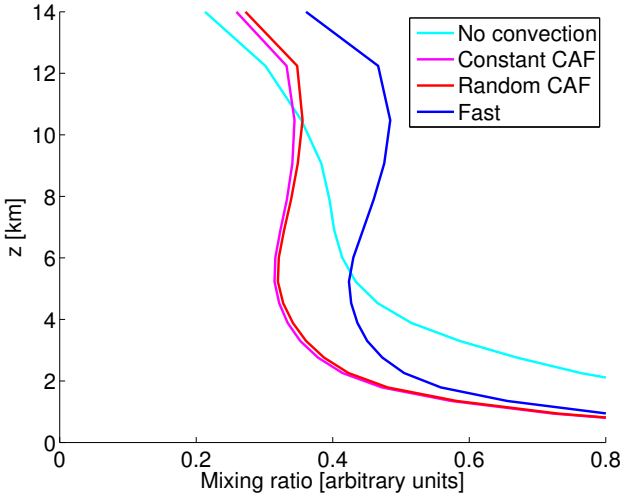

Figure 15. Mean simulated artificial SO_2-like tracer profiles in the tropics (30° S–30° N) for a run without convection, a run with a constant convective area fraction profile, a run with a random convective area fraction profile and a run where the vertical updraft velocity is set to a constant value of 100 $\mathrm{m/s}$ to mimic the almost instantaneous redistribution in other Lagrangian convective transport schemes.

scheme is robust with respect to the exact parameterization of the vertical updraft velocities, as long as the order of magnitude of the velocities is right.

6 Conclusions

We present a newly developed Lagrangian convective transport scheme for Chemistry and Transport Models and ensemble trajectory simulations. The scheme is driven by convective mass fluxes and detrainment rates from meteorological data or General Circulation Models and relies on an external convective parameterization. Our scheme extends the usual approach used in Lagrangian models of statistically redistributing air parcels within a fixed time step by modelling the time that an air parcels spends inside the convective event. This is important for correctly simulating the chemistry of short-lived species in the troposphere and may be crucial for determining their mixing ratios in the upper troposphere (e.g. Hoyle et al., 2011). As an example, we show that there is a significant effect on the mixing ratios of SO_2 when using our scheme compared to a scheme with a nearly instantenous redistribution of air parcels (see Figure 15).

Runs are performed with the convective transport model implemented into the ATLAS Chemistry and Transport Model (e.g. Wohltmann and Rex, 2009) and are driven by ECMWF ERA Interim reanalysis (Dee et al., 2011).

The algorithm is successfully validated by showing that the scheme is able to reproduce the convective mass fluxes and detrainment rates from the meteorological data within a few percent. Mass conservation in a global 15 year trajectory simulation is also within a few percent, with no apparent trend.

Two parameterizations for the vertical updraft velocities are tested and compared to wind profiler measurements conducted at Darwin, Australia. The two parameterizations use either a constant or a random convective area fraction profile. Frequency distributions of the modelled vertical velocities agree well with the measurements for the random convective area fraction method and vertical velocities larger than $0.6\,\mathrm{m/s}$, but show some discrepancies for small vertical velocities or the constant convective area fraction method. However, it turns out that it is a favorable property of the scheme that the results for chemical tracers are robust with respect to the exact parameterization of the vertical updraft velocities, as long as the order of magnitude of the velocities is right.

Global long-term trajectory simulations of Radon-222 driven by the ECMWF ERA Interim reananlysis and using the convective transport scheme are performed to examine how well the model compares to observations. The runs show a reasonable agreement to the measurements. It is however difficult to draw clear conclusions from the validation with these measurement data due to the large uncertainties in emissions, the limited amount of measurements and the dependence on the used meteorological data used by the convective transport scheme.

Future work will include e.g. the simulation of downdrafts and improvements in the mid-latitudes. For this work, we largely concentrated on the performance in the tropics, the region of the first application cases.

So far, the scheme has been applied in the calculation of the origin and convective properties of air sampled during flights of the StratoClim campaign, and has been used for transport and chemistry calculations of SO_2 to determine the contribution of SO_2 to the stratospheric sulfur burden. These application cases will be presented in separate studies.

Code and data availability. The source code is available on the AWIForge repository (https://swrepo1.awi.de/). Access to the repository is granted on request under the given correspondence address. Radon climatological profile over land for the NH mid-latitude region was obtained from Liu et al. (1984). The aircraft Radon measurements of the Moffett field and NARE data are available from the Table 1 in Kritz et al. (1998) and Table 3 in Zaucker et al. (1996) respectively. Vertical wind profiler data are available upon request to Alain Protat (alain.protat@bom.gov.au).

Author contributions. IW and RL developed and validated the convection model. MR initiated the model development and contributed to the discussion. GG and KP provided the stochastic model for the convective area fraction and contributed to the discussion. WF contributed to the discussion and provided the Radon data. AP provided the Darwin wind profiler data and contributed to the analysis of the vertical velocity comparisons. VL provided the CPOL cloud top heights extracted over the Drawin profiler site. CW produced the dual-frequency vertical air velocity retrievals.

Competing interests. The authors declare that they have no conflict of interest.

Geosci. Model Dev. Discuss., https://doi.org/10.5194/gmd-2019-5
Manuscript under review for journal Geosci. Model Dev.
Discussion started: 5 February 2019

Acknowledgements. This research has received funding from the European Community's Seventh Framework Programme (FP7/2007–2013) under grant agreement no. 603557 (StratoClim). We thank ECMWF for providing reanalysis data and Holger Deckelmann for his support in handling and obtaining the ECMWF data. Thanks go to Benjamin Segger for his work on Figures 1 and 2.

Geosci. Model Dev. Discuss., https://doi.org/10.5194/gmd-2019-5
Manuscript under review for journal Geosci. Model Dev.
Discussion started: 5 February 2019

References

Arakawa, A.: The cumulus parameterization problem: past, present, and future, J. Clim., 17, 2493–2525, 2004.

Bechtold, P., Chaboureau, J.-P., Beljaars, A., Betts, A. K., Köhler, M., Miller, M., and Redelsperger, J.-L.: The simulation of the diurnal cycle of convective precipitation over land in a global model, Quart. J. Roy. Meteorol. Soc., 130, 3119–3137, 2004.

Berglen, T. F., Berntsen, T. K., Isaksen, I. S. A., and Sundet, J. K.: A global model of the coupled sulfur/oxidant chemistry in the troposphere: The sulfur cycle, J. Geophys. Res., 109, D19310, https://doi.org/10.1029/2003JD003948, 2004.

Collins, W. J., Derwent, R. G., Johnson, C. E., and Stevenson, D. S.: A comparison of two schemes for the convective transport of chemical species in a Lagrangian global chemistry model, Quart. J. Roy. Meteorol. Soc., 128, 991–1009, 2002.

Davies, L., Jakob, C., May, P., Kumar, V. V., and Xie, S.: Relationships between the large-scale atmosphere and the small-scale convective state for Darwin, Australia, J. Geophys. Res., 118, 11,534–11,545, https://doi.org/10.1002/jgrd.50645, 2013.

Dee, D. P., Uppala, S. M., Simmons, A. J., Berrisford, P., Poli, P., Kobayashi, S., Andrae, U., Balmaseda, M. A., Balsamo, G., Bauer, P., Bechtold, P., Beljaars, A. C. M., van de Berg, L., Bidlot, J., Bormann, N., Delsol, C., Dragani, R., Fuentes, M., Geer, A. J., Haimberger, L., Healy, S. B., Hersbach, H., Hólm, E. V., Isaksen, L., Kållberg, P., Köhler, M., Matricardi, M., McNally, A. P., Monge-Sanz, B. M., Morcrette, J.-J., Park, B.-K., Peubey, C., de Rosnay, P., Tavolato, C., Thépaut, J.-N., and Vitart, F.: The ERA-Interim reanalysis: configuration and performance of the data assimilation system, Q. J. R. Meteorol. Soc., 137, 553–597, 2011.

Feng, W., Chipperfield, M. P., Dhomse, S., Monge-Sanz, B. M., Yang, X., Zhang, K., and Ramonet, M.: Evaluation of cloud convection and tracer transport in a three-dimensional chemical transport model, Atmos. Chem. Phys., 11, 5783–5803, 2011.

Forster, C., Stohl, A., and Seibert, P.: Parameterization of convective transport in a Lagrangian particle dispersion model and its evaluation, J. Appl. Meteorol. Clim., 46, 403–422, 2007.

Gottwald, G. A., Peters, K., and Davies, L.: A data-driven method for the stochastic parametrisation of subgrid-scale tropical convective area fraction, Quart. J. Roy. Meteorol. Soc., 142, 349–359, 2016.

Heymsfield, G. M., Tian, L., Heymsfield, A. J., Li, L., and Guimond, S.: Characteristics of deep tropical and subtropical convection from nadir-viewing high-altitude airborne Doppler radar, J. Atmos. Sci., 67, 285–308, 2010.

Hoyle, C. R., Marécal, V., Russo, M. R., Allen, G., Arteta, J., Chemel, C., Chipperfield, M. P., D'Amato, F., Dessens, O., Feng, W., Hamilton, J. F., Harris, N. R. P., Hosking, J. S., Lewis, A. C., Morgenstern, O., Peter, T., Pyle, J. A., Reddmann, T., Richards, N. A. D., Telford, P. J., Tian, W., Viciani, S., Volz-Thomas, A., Wild, O., Yang, X., and Zeng, G.: Representation of tropical deep convection in atmospheric models – Part 2: Tracer transport, Atmos. Chem. Phys., 11, 8103–8131, 2011.

Jacob, D. J., Prather, M. J., Rasch, P. J., Shia, R.-L., Balkanski, Y. J., Beagley, S. R., Bergmann, D. J., Blackshear, W. T., Brown, M., Chiba, M., Chipperfield, M. P., de Grandpré, J., Dignon, J. E., Feichter, J., Genthon, C., Grose, W. L., Kasibhatla, P. S., Köhler, I., Kritz, M. A., Law, K., Penner, J. E., Ramonet, M., Reeves, C. E., Rotman, D. A., Stockwell, D. Z., Velthoven, P. F. J. V., Verver, G., Wild, O., Yang, H., and Zimmermann, P.: Evaluation and intercomparison of global atmospheric transport models using ^{222}Rn and other short-lived tracers, J. Geophys. Res., 102, 5953–5970, 1997.

Kritz, M. A., Rosner, S. W., and Stockwell, D. Z.: Validation of an off-line three-dimensional chemical transport model using observed radon profiles: 1. Observations, J. Geophys. Res., 103, 8425–8432, 1998.

Kumar, V. V., Jakob, C., Protat, A., Williams, C. R., and May, P. T.: Mass-Flux characteristics of tropical cumulus clouds from wind profiler observations at Darwin, Australia, J. Atmos. Sci., 72, 1837–1855, 2015.

Lelieveld, J.: Multi-Phase Processes in the Atmospheric Sulfur Cycle, in: Interactions of C, N, P and S Biogeochemical Cycles and Global Change, edited by Wollast, R., Mackenzie, F. T., and Chou, L., pp. 305–331, Springer, New York, 1993.

LeMone, M. A. and Zipser, E. J.: Cumulonimbus vertical velocity events in GATE. Part I: Diameter, intensity and mass flux, J. Atmos. Sci., 37, 2444–2457, 1980.

Liu, S. C., McAfee, J. R., and Cicerone, R. J.: Radon 222 and tropospheric vertical transport, J. Geophys. Res., 89, 7219–7292, 1984.

Mahowald, N. M., Rasch, P. J., and Prinn, R. G.: Cumulus parameterizations in chemical transport models, J. Geophys. Res., 100, 26 173–26 189, 1995.

May, P. T. and Rajopadhyaya, D. K.: Vertical velocity characteristics of deep convection over Darwin, Australia, Mon. Weather Rev., 127, 1056–1071, 1999.

Peters, K., Jakob, C., Davies, L., Khouider, B., and Majda, A. J.: Stochastic Behavior of Tropical Convection in Observations and a Multicloud Model, J. Atmos. Sci., 70, 3556–3575, https://doi.org/10.1175/JAS-D-13-031.1, 2013.

Rex, M., Wohltmann, I., Ridder, T., Lehmann, R., Rosenlof, K., Wennberg, P., Weisenstein, D., Notholt, J., Krüger, K., Mohr, V., and Tegtmeier, S.: A tropical West Pacific OH minimum and implications for stratospheric composition, Atmos. Chem. Phys., 14, 4827–4841, 2014.

Rossi, D., Maurizi, A., and Fantini, M.: IL-GLOBO (1.0) – development and verification of the moist convection module, Geosci. Model Dev., 9, 789–797, 2016.

Taszarek, M., Brooks, H. E., Czernecki, B., Szuster, P., and Fortuniak, K.: Climatological Aspects of Convective Parameters over Europe: A Comparison of ERA-Interim and Sounding Data, J. Clim., 31, 4281–4308, 2018.

Tiedtke, M.: A comprehensive mass flux scheme for cumulus parameterization in large-scale mdoels, Mon. Wea. Rev., 117, 1779–1800, 1989.

Tsai, L.-C., Chen, J.-P., Lin, P.-Y., Wang, W.-C., and Isaksen, I. S. A.: Sulfur cycle and sulfate radiative forcing simulated from a coupled global climate-chemistry model, Atmos. Chem. Phys., 10, 3693–3709, 2010.

Williams, C. R.: Vertical air motion retrieved from dual-frequency profiler observations, J. Atmos. Oceanic Technol., 29, 1471–1480, 2012.

Wohltmann, I. and Rex, M.: The Lagrangian chemistry and transport model ATLAS: validation of advective transport and mixing, Geosci. Model Dev., 2, 153–173, 2009.

Zaucker, F., Daum, P. H., Wetterauer, U., Berkowitz, C., Kromer, B., and Broecker, W. S.: Atmospheric ^{222}Rn measurements during the 1993 NARE Intensive, J. Geophys. Res., 101, 29 149–29 164, 1996.